Article

Influence of Reservoir Stimulation on Marine Gas Hydrate Conversion Efficiency in Different Accumulation Conditions

Lin Yang [1,2,3,4], Chen Chen [1,2,3,4,*], Rui Jia [1,2,3,4,*], Youhong Sun [1,2,3,4], Wei Guo [1,2,3,4], Dongbin Pan [1,2,3,4], Xitong Li [1,2,3,4] and Yong Chen [1,2,3,4]

[1] Engineering College, Jilin University, Changchun 130026, China; yanglin14@mails.jlu.edu.cn (Y.L.); chenchen@jlu.edu.cn (C.C.); jiarui@jlu.edu.cn (J.R.); syh@jlu.edu.cn (S.Y.); guowei6981@jlu.edu.cn (G.W.); pandb16@mails.jlu.edu.cn (P.D.); lixt15@mails.jlu.edu.cn (L.X.); chenyong15@mails.jlu.edu.cn (C.Y.)
[2] State Key Laboratory of Superhard Materials, Changchun 130012, China
[3] Key Laboratory of Drilling and Exploitation Technology in Complex Conditions, Ministry of Land and Resources, Changchun 130026, China
[4] National Geophysical Exploration Equipment Engineering Research Center, Jilin University, Changchun 130026, China
* Correspondence: chenchen@jlu.edu.cn (C.C.); Tel.: +86-0431-88502678 (C.C.)
jiarui@jlu.edu.cn (J.R.); +86-0431-88502678 (J.R.)

Abstract: Based on the geologic conditions of natural gas hydrate (NGH) accumulations in the Shenhu area, northern slope of the South China Sea, this paper used a method of combining reservoir stimulation technique (RST) with depressurization to investigate the conversion efficiency of marine NGH reservoirs in different intrinsic permeability and initial NGH saturation conditions, and analyze the influence of variably-stimulation effect on marine NGH conversion efficiency in different accumulation conditions, provided a reference scheme for improving the NGH conversion efficiency in the Shenhu area. In this work, we performed calculations for the variations in CH_4 production rate and cumulative volume of CH_4 in different initial NGH saturation, intrinsic permeability and stimulation effect conditions, variance analysis and range analysis methods were used to analyze the significance of these key factors and their interaction, and investigated the sensitivity of stimulation effect on NGH conversion efficiency, respectively. The simulation results showed that stimulation effect have a significant influence on NGH conversion efficiency, and the influence of interaction between these three factors were not obvious. Possibly most important, we clarified an optimum stimulation effect for higher NGH conversion efficiency under different accumulation conditions, especially in low-permeability and high-saturation, which corresponding stimulation effect were different.

Keywords: natural gas hydrate; reservoir stimulation technique; variance analysis; conversion efficiency; sensitivity analysis; numerical simulation

---

Nomenclature:

TCF	Trillion cubic feet, 1 Tcf = 283.17 × 10^9 m^3	
z	position of HBL below ocean surface	(m)
Z_H	HBL thickness	(m)
H_1	Depth of HBL below seafloor	(m)
H_2	Depth of seafloor	(m)
H_w	Production well length	(m)
G	Thermal gradient below seafloor	(°C/m)
P_0	Initial pressure (at base of HBL)	(MPa)
ΔP	Production pressure	(MPa)
P_{cap}	Capillary pressure	(MPa)

Peer-reviewed version available at Energies 2018, 11, 339; doi:10.3390/en11020339

P_{01}	Atmosphere pressure	(Pa)
T_0	Initial temperature (at base of HBL)	(°C)
k_x, k_y, k_z	Intrinsic permeability	(md)
k_c	Permeability of fracturing cracks (h_2 = 10 mm)	(md)
k_{rA}	Aqueous relative permeability	(md)
k_{rG}	Gas relative permeability	(md)
K_{dry}	Dry thermal conductivity	(W/(kg·°C))
K_{wet}	Wet thermal conductivity	(W/(kg·°C))
K_Θ	Thermal conductivity	(W/(kg·°C))
Φ	Porosity	
ρ_R	Grain density	(kg/m³)
S_H	Saturation of natural gas hydrate	
S_A	Saturation of aqueous	
r	Radius	(m)
Xs	Salinity	
λ	Van Genuchten exponent—Table 2	
h	Crack height	(mm)
L_f	Crack length	(m)
Δl	Crack spacing	(m)

Subscripts and Superscripts:

A	Aqueous phase
B	Base of HBL
cap	Capillary
G	Gas phase
HBL	Hydrate-bear layer
irA	Irreducible aqueous phase
irG	Irreducible gas
N	Permeability reduction exponent—Table 2
n_G	Gas permeability reduction exponent—Table 2
OB	Overburden
UB	Underburden

1. Introduction

1.1. Background

Natural gas hydrates (NGH) are white and pale yellow, solid, ice-like cage type crystalline compounds [1], formed by small molecule gases such as light hydrocarbons, carbon dioxide and water under low temperature and high pressure conditions, and also known as "combustible ice" [2]. About 90% of marine sediments are satisfied the favorable temperature and pressure conditions of NGH formation and stability [3]. NGH has a low environmental risk, in the standard state, each unit volume of methane hydrate decomposition, about 164 volumes of methane was produced [4]. Very clean natural gas can be produced from NGH deposits, especially from sandy turbidites, from which it is already known in the industry how to produce conventional hydrocarbons [5]. It is estimated that natural gas from NGH in sands are >40,000 Tcf [6,7]. NGH should be converted in situ to its constituent gas and water [8]. A number of conversion methods exist [9,10], but early production testing and modeling indicate that depressurization will be the ideal method to use [11,12].

NGH enrichment area of the Shenhu area is located in the northern slope of the South China Sea, between Xisha Trough and Dongsha Islands (Fig. 1) [13,14]. In NGH enrichment area, it is characterized by large thickness of sedimentary formations, rich contents of organic matter and high sedimentation, the thermogenic gas originated from deep formations and microbial and thermogenic gases originated from the shallow formations provided sufficient gas source to the formation of NGH [15,16]. In this area, the water depth is 1000–1700m [17]. The temperature of ocean floor, heat flow,

Preprints (www.preprints.org) | NOT PEER-REVIEWED | Posted: 11 December 2017 doi:10.20944/preprints201712.0062.v1

Peer-reviewed version available at *Energies* **2018**, *11*, 339; doi:10.3390/en11020339

geothermal gradient and organic matter contents are 3.3–3.7 °C, 74.0–78.0 mW/m², 43–67.7 °C/km and 0.46%–1.4%, respectively, which satisfied the favorable geological and thermodynamic conditions of NGH formation and stability [14,15,18,19].

1.2. Hydrates in the Shenhu Area

In 2007, NGH samples were successfully drilled from the SH2, SH3, and SH7 sites of GMGS-1 research area in the Shenhu area, the northern South China Sea (Fig. 1) [14]. The drilling results showed that the top of the hydrate-bearing layers (HBL) are located at 115–229 m below the ocean floor [14,15]. In 2015, a total of 19 sites, 23 wells were drilled in GMGS-3 research area in the Shenhu area in the northern South China Sea (Fig. 1) [15,20,21]. The well logging data showed that all of these stations were found NGH, and NGH samples were collected in four of these wells. The hydrate layers are 13–70m thick, and the NGH saturation are 13%–53%, and in local regions, NGH saturation up to 75%. [15,20]. The exploration results of GMGS-1 and GMGS-3 showed that the NGH enrichment area in the Shenhu area hold large NGH reserves, however, NGH saturations and permeability of reservoirs are clear difference both in horizontal and vertical directions, and strong heterogeneity [20]. Table 1 showed the characteristics of the NGH deposits with greater exploitation potential.

Table 1. The characteristics of the NGH deposits with greater exploitation potential.

Group	HBL thick / m	Range of S_{H0}	Average S_{H0}	k / md
SH2	43	0 – 48%	21%	10
SH7	18 - 34	20% - 44%	41%	75
W02	24	–	13.7%	–
W07	20	45% - 75%	50%	22 – 40
W11	>70	21% - 53%	40%	–
W17	45	–	19.4%	–
W19	68	17% - 64%	45.2%	5.5

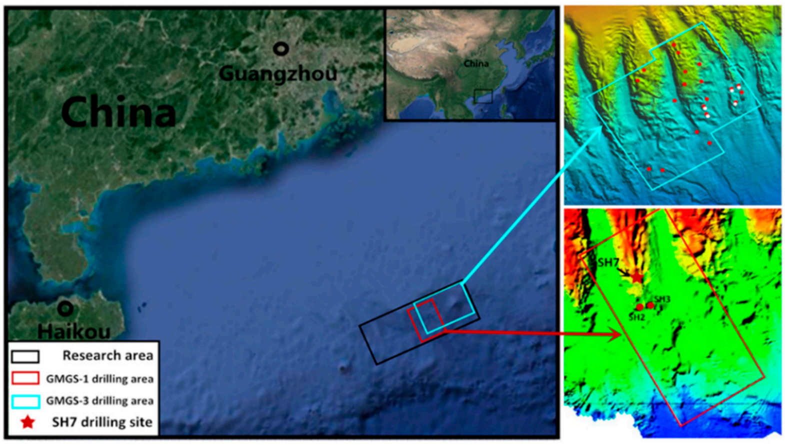

Fig. 1. Location of the research area and drilling sites in the Shenhu area, northern slope of the South China Sea.

Peer-reviewed version available at Energies 2018, 11, 339; doi:10.3390/en11020339

1.3. Significance and Feasibility of Stimulation for Marine NGH Reservoir

NGH are mainly stored in sandy and silty marine sediments. Clay and clastic limestone and secondary permeability related to structure also host NGH in some areas of the South China Sea [18]. The NGH-enriched reservoirs in the Shenhu area, with a poor permeability, which hinder the transfer of heat and pressure between the production wells and the reservoir, and reduces the conversion efficiency of the continuous dissociation of NGH [14,22,23]. The problem of how to efficiently and economically exploit natural gas hydrate in low-permeability marine sediment reservoirs is an important issue. Being able to exploit NGH from marine sediments, especially in low-permeability silt and clay sediments with a less producible capacity, will greatly enlarge the potential use of NGH as a gas resource [23].

The reservoir stimulation technique (RST) is to stimulate the reservoir by fracturing [24]. RST is aimed at fracturing more main cracks and multi-level secondary cracks, to form a fractured network system. Realizing the communication between main cracks and natural cracks at the same time [25]. "Breaking up" the effective reservoir to increase the contact area between cracks wall and reservoir, and reduce the seepage distance from effective reservoir to cracks, would be greatly improved the permeability of reservoir [26,27]. RST has expanded to include low-permeability oil and gas shale, as well as tight sand reservoirs [28]. Depressurization method and RST combine to exploit NGH, which will increase the transmission rate of depressurization within NGH deposit and promote NGH decomposition in fractured zones, in addition, being conducive to the discharge of methane [23,29-31].

The formation of NGH in host sediment pore space results in a higher bulk modulus and increased mechanical strength [4,6]. In an ideal case, a hydrate deposit was probably had a sufficient brittle response to fracturing, our model would provide a base case with which actual testing can be compared in order to assess the likelihood of artificial fracturing of inducing additional permeability in semi-consolidated marine sediments, which, without NGH, would be expected to respond in a more mechanically-ductile manner [23].

1.4. Objetive

The main objective of this study is to investigate the influence of RST on the conversion efficiency of NGH under different accumulation conditions such as initial NGH saturation, intrinsic permeability and variably-stimulation effect by depressurization method. Provided a reference program for increasing NGH conversion efficiency of NGH accumulations from the Shenhu area, the northern South China Sea, in different permeability and saturation conditions, especially in low-permeability and high-saturation.

2. Materials and Methods

2.1. Numerical Model and Simulation Parameters

2.1.1. Numerical Simulation Code

The simulator model used in this work was TOUGH+HYDRATE v1.0, it is a numerical simulator developed by Moridis from the Lawrence Berkeley National Laboratory (Berkeley, CA, USA), and the first member of TOUGH+, and the successor to TOUGH2. The model can simulate the formation and decomposition of natural gas hydrate, phase equilibrium, seepage, and heat and mass transfer processes under complex conditions and non-isothermal conditions. In addition, the model can simulate production from natural CH_4-hydrate deposits in the subsurface (i.e., in permafrost and

Peer-reviewed version available at *Energies* **2018**, *11*, 339; doi:10.3390/en11020339

deep ocean sediments) as well as laboratory experiments of hydrate dissociation and formation in porous and fractured media, using the methods of depressurization, heating injection, and injection inhibition [32]. In recent years, TOUGH+HYDRATE v1.0 models have been widely used in NGH simulations. Li, et al. [14] used this model to evaluate NGH conversion potential by depressurization and thermal stimulation from the SH7 site. Su, et al. [22] used depressurization and thermal stimulation method to analyze NGH conversion efficiency from the SH2 site. Chen, et al. [23] used this model to investigate the effect of fracturing technology on the production efficiency of NGH by depressurization from the SH7 site.

2.1.2. System Parameters and Initialization of the Model

The geologic system used in this study was according to the drilling results of GMGS-1 and GMGS-3 in the Shenhu area, the northern South China Sea. The hydrate samples from this area were dominated by methane hydrate, in some areas, were almost pure methane hydrate (99.2%) [14]. Therefore, only methane hydrate was simulated. The system parameters, part of initial conditions and mathematical models of the simulation were shown in Table 2. The main parameters in the simulation were derived from the previous literature on NGH reservoirs in this area [14,20,23].

Table 2. Production trial properties and mathematical models.

Parameter	Value	Parameter	Value
Initial pressure P_0 (at base of HBL)	13.83 Mpa	Composite thermal conductivity model [32,33]	$K_\theta = K_{dry} + \left(\sqrt{S_A} + \sqrt{S_H}\right)\left(K_{wet} - K_{dry}\right) + \alpha S_I K_I$
Initial temperature T_0 (at base of HBL)	14.15 °C		
Depth of seafloor	1108 m	Capillary pressure model [34]	$P_{cap} = -P_{01}\left[(S^*)^{-1/\lambda} - 1\right]^{1-\lambda}$
Thermal gradient	0.0433 °C/m		$S^* = (S_A - S_{irA})/(S_{mxA} - S_{irA})$
HBL thickness Z_H	22 m	S_{irA}	0.29
Production well length H_w	6 m	λ	0.45
Depth of HBL H_1	155–177 m	P_{01}	10^5 Pa
Gas composition	100% CH_4	Relative permeability model [32]	$K_{rA} = (S^*)^n$
Porosity Φ	0.38		$K_{rG} = ({S_G}^*)^{n_G}$
Grain density ρ_R	2600 kg/m³		EPM #2 model
Water salinity (mass fraction) Xs	0.0305	N	3.572
Dry thermal conductivity K_{dry}	1.0 W/(kg·°C)	n_G	3.572
Wet thermal conductivity K_{wet}	3.1 W/(kg·°C)	S_{irA}	0.30
Production pressure P_w	$0.5P_0$	S_{irG}	0.05

2.2. Design of the Production Well and Reservoir Stimulation Cracks

2.2.1. Production Well Design

In this paper, a single vertical well which had a 6m height production interval was located in the middle of NGH deposit with a radius of r_w = 0.1 m was used, and the simulation system was cylindrical (Fig. 2A). The production interval design referred to Su [22] and Li [35]'s studies. Setting the production well in the middle of NGH deposit was to reduce natural gas spillage through overburden (OB) and underburden (UB).

Peer-reviewed version available at *Energies* **2018**, *11*, 339; doi:10.3390/en11020339

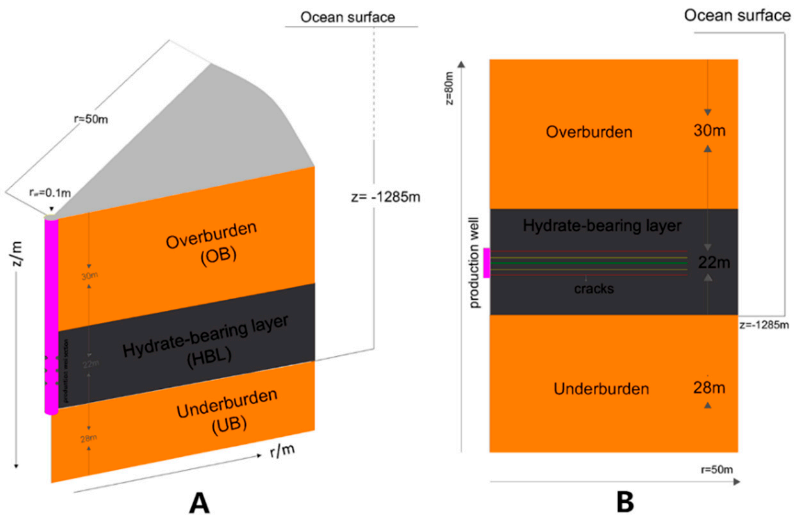

Fig. 2. (A) Design of the production well design, and (B) Diagram of the horizontal stimulation cracks.

2.2.2. Stimulated Cracks Design

Reservoir stimulation was a complex process, the fracturing cracks morphology were affected by a lot of parameters such as the physical and mechanical properties of the formation, the stress distribution of target formation, and so on, complex and difficult to descript [23]. Therefore, in this work, in order to simplify the physical model, the fractured network system was simplified into multiple horizontal cracks. With different crack densities to represent the different stimulation effect, the larger crack quantity and smaller crack spacing represent the better stimulation effect, with dense fractured network in fracturing zone. Under the opposite conditions, represent the poor stimulation effect, with sparse fractured network in fracturing zone. According to the different stimulation effect, the cracks were divided into spacing categories, Δl = 3 m, 2m, 1m, respectively, for three, four, and five cracks, and these cracks were uniformly distributed in production well, which increased the communication between production well and NGH deposit. The parameters of cracks were showed in Table 3. And the crack length was L_f = 40 m, and crack height was h = 10 mm, as shown in Fig. 2B.

Table 3. Parameters of cracks.

Parameter	Value of Cracks
Crack quantity	3, 4, 5
Crack spacing Δl	3 m (three cracks), 2 m (four cracks) 1 m (five cracks)
permeability k_0	520md

The permeability of the cracks varied according to the porosity. The porosity and permeability have the following relationships [36-38]:

$$\frac{k}{k_0} = F_{\Phi S} = \left(\frac{\Phi}{\Phi_0}\right)^n \tag{2-1}$$

$$\frac{k}{k_0} = F_{\Phi S} = \left(\frac{\Phi - \Phi_c}{\Phi_0 - \Phi_c}\right)^n \tag{2-2}$$

Where k_0 is the formation permeability, k is the formation permeability after the porosity change, Φ_0 is the formation porosity, Φ is the porosity of the formation after the change, and Φ_c is a non-zero critical porosity. In Equation (2-1), n is 2 or 3; in Equation (2-2), n is 10 or more.

Preprints (www.preprints.org) | NOT PEER-REVIEWED | Posted: 11 December 2017 doi:10.20944/preprints201712.0062.v1

Peer-reviewed version available at *Energies* **2018**, *11*, 339; doi:10.3390/en11020339

3. Simulation Experiment Results and Discussion

3.1. Factors significance and influence rules analysis

In this work, we considered the interaction of various factors and used whole simulation experiments method ($L_{27}(3)^{13}$) to analyze the significance of intrinsic permeability *k*, initial NGH saturation S_{H0} and stimulation effect (represented by cracks quantity *N*) and their interaction on NGH conversion efficiency of NGH deposits in the Shenhu area. Because these factors and their interactions both would affect NGH conversion efficiency, it was inaccurate to use a single variable approach to describe the influence rules of these three factors on NGH conversion efficiency, a whole simulation experiments program which contained the interactions between these factors was necessary. In this work, using CH_4 cumulative volume Q_{cv} to represent NGH conversion efficiency, the depressurization exploitation time was set to five years, because the CH_4 production rates were stabilized at this time.

Table 4. The simulation experiments factor level table.

Level	Factor		
	intrinsic permeability *k*	initial NGH saturation S_{H0}	cracks quantity *N*
1	7.5mD	0.3	3
2	40mD	0.4	4
3	75mD	0.5	5

Table 4 showed the levels of these three key factors, and Table 5 showed the 3^3 whole simulation experiments program and the simulation experiments results. As shown in Table 5, for example, the $k \times S_{H0}$, $k \times N$ and $S_{H0} \times N$ meant the interaction column between intrinsic permeability *k* and initial NGH saturation S_{H0}, intrinsic permeability *k* and cracks quantity *N*, and initial NGH saturation S_{H0} and cracks quantity *N*, respectively, and the ninth, tenth, twelfth and thirteenth columns were used for error analysis, which were vacant columns and not written in Table 5 in this work.

Table 5. $L_{27}(3)^{13}$ whole simulation experiments program and simulation experiments results.

Test number	*k* 1	S_{H0} 2	$k \times S_{H0}$ 3	4	*N* 5	$k \times N$ 6	7	$S_{H0} \times N$ 8	11	Q_{cv} (m^3)
1	1(7.5mD)	1(0.3)	1	1	1(3)	1	1	1	1	306394.8
2	1	1	1	1	2(4)	2	2	2	2	201014.4
3	1	1	1	1	3(5)	3	3	3	3	305693.9
4	1	2(0.4)	2	2	1	1	1	2	3	159854.8
5	1	2	2	2	2	2	2	3	1	183312.3
6	1	2	2	2	3	3	3	1	2	202049.4
7	1	3(0.5)	3	3	1	1	1	3	2	154356.7
8	1	3	3	3	2	2	2	1	3	161279.1
9	1	3	3	3	3	3	3	2	1	208541.0
10	2(40mD)	1	2	3	1	2	3	1	1	697573.4
11	2	1	2	3	2	3	1	2	2	615799.1
12	2	1	2	3	3	1	2	3	3	692369.2
13	2	2	3	1	1	2	3	2	3	643712.3
14	2	2	3	1	2	3	1	3	1	541653.4
15	2	2	3	1	3	1	2	1	2	618998.9
16	2	3	1	2	1	2	3	3	2	473955.6
17	2	3	1	2	2	3	1	1	3	465767.0
18	2	3	1	2	3	1	2	2	1	531254.1
19	3(75mD)	1	3	2	1	3	2	1	1	964843.5
20	3	1	3	2	2	1	3	2	2	901046.6

Preprints (www.preprints.org) | NOT PEER-REVIEWED | Posted: 11 December 2017 doi:10.20944/preprints201712.0062.v1

Peer-reviewed version available at Energies 2018, 11, 339; doi:10.3390/en11020339

21	3	1	3	2	3	2	1	3	3	1025723.8
22	3	2	1	3	1	3	2	2	3	898493.9
23	3	2	1	3	2	1	3	3	1	792966.1
24	3	2	1	3	3	2	1	1	2	939190.8
25	3	3	2	1	1	3	2	3	2	835660.1
26	3	3	2	1	2	1	3	1	3	688925.5
27	3	3	2	1	3	2	1	2	1	737725.1
T										1.493×10^{7}
$\overline{x_{1-cv}}$	211589.9	634495.4			570538.3					
$\overline{x_{2-cv}}$	582270.1	552043.6			505751.5					
$\overline{x_{3-cv}}$	864952.8	472273.8			582523.0					

As shown in Table 5, $\bar{x}$ was the average value of the same level of each factor. As shown in Table 6, analysis of variance was applied to analysis the significance and sensitivity of these three factors on NGH conversion efficiency. In these two tables,

$$SS_T = \sum {Q_{cv}}^2 - C,\ C = T_{cv}^2/n \tag{3-1}$$

$$SS_{i=k,SH0,N,k\times SH0,k\times N\ and\ SH0\times N} = \sum \frac{{T_i}^2}{K_i} - C, \tag{3-2}$$

$$SS_e = SS_T - \sum SS_i \tag{3-3}$$

Where, SS_T was total sum of square, C was correction parameter, n was test quantity and n=27. In equation 3-2 and 3-3, SS_i were the sum of square of each factor and SS_e was the error sum of square, the number of repetitions of each factor K_i =9.

$$df_T = \text{n-1} \tag{3-4}$$

$$df_{j=k,\,SH0,\,N} = x_j - 1,\ x_j = 3 \tag{3-5}$$

$$df_{m=k\times SH0,\,k\times N,\,SH0\times N} = df_k + df_{SH0} = df_k + df_N = df_{SH0} + df_N \tag{3-6}$$

$$df_e = df_T - \sum df_j - \sum df_m \tag{3-7}$$

$$MS = SS/df \tag{3-8}$$

$$F = \frac{SS_i/df_i}{SS_e/df_e} \tag{3-9}$$

Where, df_T was the total degree of freedom, df_e was degree of freedom for error, $df_{j,m}$ were degree of freedom for factors j and m, x_j were the levels of each factor and MS was mean square. $F_{0.05(2,8)}$ and $F_{0.01(2,8)}$ were derived from the standard $F(f_1,f_2)$ table.

By comparing F_i and $F_{0.05(2,8)}$ and $F_{0.01(2,8)}$, the impact of factor i was significant when $F_i > F_{0.05(2,8)}$, and had a more significant influence when $F_i > F_{0.01(2,8)}$. As shown in Table 6, $F_k > F_{SH0} > F_{0.05(2,8)} > F_{0.01(2,8)}$, which meant intrinsic permeability k and initial NGH saturation S_{H0} had a more significant influence on CH_4 cumulative volume. And $F_{0.01(2,8)} > F_N > F_{0.05(2,8)}$, crack quantity N had a significant influence on CH_4 cumulative volume, which was smaller than that of k and S_{H0}, the significance of interaction between k, S_{H0} and N were small. The results showed that the impact of intrinsic permeability, initial NGH saturation and stimulation effect on NGH conversion efficiency were significant, however, the interaction had no significant effect.

Peer-reviewed version available at Energies 2018, 11, 339; doi:10.3390/en11020339

Table 6. Analysis of variance of Q_{cv}

Parameters	*SS*	*df*	*MS*	*F*	$F_{0.05(2,8)}$	$F_{0.01(2,8)}$	Significance
k	1.933×10^{12}	2	9.663×10^{11}	506.59	4.46	8.65	***
S_{H0}	1.118×10^{11}	2	5.921×10^{10}	31.04	4.46	8.65	**
N	3.070×10^{10}	2	1.535×10^{10}	8.05	4.46	8.65	*
$k \times S_{H0}$	1.246×10^{10}	4	3.114×10^{9}	1.63			
$k \times N$	5.695×10^{9}	4	1.424×10^{9}	0.75			
$S_{H0} \times N$	2.028×10^{9}	4	5.069×10^{8}	0.27			
Error (e)	1.526×10^{10}	8	1.907×10^{9}				
Total (T)	2.117×10^{12}	26					

In order to identify the influence rules of each factor for NGH conversion efficiency, multiple comparisons of the three factors were used. As shown in Table 7, Table 8 and Table 9, by comparing $\overline{x_{cv}}$ of each level, the results showed, for intrinsic permeability k, NGH conversion efficiency was substantial increased with increasing k, however, the growth rate was decreasing. For initial NGH saturation S_{H0}, a lower S_{H0} led to a higher NGH conversion efficiency, and the reduction rate was decreasing. For crack quantity N, dense fractured network had a higher NGH conversion efficiency, but the impact of sparse fractured network was slightly less than that of dense fractured network. By comparing the difference between the maximum and minimum $\overline{x_{cv}}$ of each level, it was showed that the influence on NGH conversion efficiency was increased by about 4 times, in comparison with S_{H0} and k.

Table 7. Multiple comparison of factor k.

Factor k	$\overline{x_{cv}}$	$\overline{x_{3-cv}}$-211589.9	$\overline{x_{3-cv}}$-582270.1
k_3	864952.8	653362.9 **	282682.7 *
k_2	582270.1	370680.2 **	
k_1	211589.9		

Table 8. Multiple comparison of factor S_{H0}.

Factor S_{H0}	$\overline{x_{cv}}$	$\overline{x_{1-cv}}$-472273.8	$\overline{x_{1-cv}}$-552043.6
S_{H01}	634495.4	162221.6 **	82451.8 **
S_{H02}	552043.6	79769.8 *	
S_{H03}	472273.8		

Table 9. Multiple comparison of factor N.

Factor N	$\overline{x_{cv}}$	$\overline{x_{3-cv}}$-505751.5	$\overline{x_{3-cv}}$-570538.3
N_3	582523.0	76771.5 **	11984.7 *
N_1	570538.3	64786.8 **	
N_2	505751.5		

3.2. Sensitivity to stimulation effect

3.2.1. Analyzed by Range Analysis Method

As shown in Table 6, the sensitivity of stimulation effect (represented by crack quantity N) on cumulative volume of CH_4 was significant. In order to investigate the influence rules of stimulation effect on NGH conversion efficiency, by meant of range analysis method, we compared the values of CH_4 cumulative volume Q_{cv} under different stimulation effect, as shown in Table 10 and Table 11.

Where, $\overline{x_{cv}}$ was the average value of CH_4 cumulative volume Q_{cv}. R_{cv} was the range of CH_4

cumulative volume Q_{cv}, and r_{cv} was rate of change between maximum $\overline{x_{cv}}$ and minimum $\overline{x_{cv}}$. Value of R_{cv} was calculated by subtracting the minimum $\bar{x}$ from the maximum $\bar{x}$, with following expression,

$$R = \overline{x_{max}} - \overline{x_{min}} \tag{3-10}$$

$$r = R / \overline{x_{min}} \tag{3-11}$$

As shown in Table 10, r_{cv} was decreased with increasing S_{H0}, and the r_{cv} for case S_{H0} = 0.3 was the largest. This was because, a higher S_{H0} had a lower effective permeability, and stimulation effect was more obvious in lower effective permeability condition, which led to a less difference of Q_{cv}. The results showed that the sensitivity of variably stimulation effect on NGH conversion efficiency was significant in low-saturation condition.

As shown in Table 11, r_{cv} for case k = 7.5 mD was much bigger than that for cases k = 40 mD and 75 mD, and r_{cv} for cases k = 40 mD and k = 75 mD were similar. This was because, RST had a greater improvement on effective permeability in lower permeability condition, and there were enough seepage channels to the discharge of methane in higher permeability condition. The results showed that the sensitivity of variably stimulation effect on NGH conversion efficiency was significant in low-permeability condition.

The influence of intrinsic permeability on sensitivity of stimulation effect on NGH conversion efficiency was bigger than that of initial NGH saturation, in comparison with r_{cv} of Table 10 and Table 11.

Table 10. Range analysis of Q_{cv} of variably N in different S_{H0} conditions.

S_{H0}	N	$\overline{x_{cv}}$ (m³) (k = 7.5mD, 40mD, 75mD)	R_{cv}	r_{cv}
	3	656270.6		
0.3	4	572620.0	101975.6	0.178
	5	674595.6		
	3	567353.7		
0.4	4	505977.3	80769.1	0.160
	5	586746.4		
	3	487990.8		
0.5	4	438657.2	53849.5	0.123
	5	492506.7		

Table 11. Range analysis of Q_{cv} of variably N in different k conditions

k/md	N	$\overline{x_{cv}}$ (m³) (S_{H0} = 0.3, 0.4, 0.5)	R_{cv}	r_{cv}
	3	271034.4		
7.5	4	181868.6	89165.8	0.490
	5	238761.4		
	3	605080.4		
40	4	541073.2	73134.2	0.135
	5	614207.4		
	3	899665.8		
75	4	794312.7	106567.1	0.134
	5	900879.8		

Preprints (www.preprints.org) | NOT PEER-REVIEWED | Posted: 11 December 2017 doi:10.20944/preprints201712.0062.v1

Peer-reviewed version available at *Energies* **2018**, *11*, 339; doi:10.3390/en11020339

3.4.2. Analyze under Low-Permeability Condition (k = 7.5 mD)

Fig. 3 showed the CH_4 production rate Q_{pr} and the cumulative volume Q_{cv} curves under low-permeability and different N conditions. In Fig. 3A, S_{H0} = 0.3. As shown in Q_{pr} curves of Fig. 3A, in the early stage of exploitation, the Q_{pr} changed greatly, then, trended to stable after about 200 days. The Q_{pr} for cases N = 3 and N = 5 were similar and much bigger than that for case N = 4. As shown in Q_{cv} curves, the Q_{cv} for cases N = 3 and N = 5 were similar and much bigger than that for case N = 4, and the Q_{cv} increased by 52.4%, in comparison with cases N = 3, N = 5 and N = 4. This was because, the cracks spacing Δl = 3m for case N = 3 was better to increase the interaction between cracks, the Q_{pr} and Q_{cv} had the largest values in this spacing under the same crack quantity condition. Also, dense fractured network had a better improvement effect under low-permeability condition.

In Fig. 3B, S_{H0} = 0.4. As shown in Q_{pr} curves of Fig. 3B, the difference of Q_{pr} were small under three crack quantity conditions, and the Q_{pr} for case N = 5 was the largest. As shown in Q_{cv} curves, the Q_{cv} for case N = 5 was the largest, and increased by 26.4%, in comparison with cases N = 3 and N = 5.

In Fig. 3C, S_{H0} = 0.5. As shown in Q_{pr} curves of Fig. 3C, in the early stage of exploitation, the Q_{pr} for case N = 5 was the biggest, and the Q_{pr} for case N = 4 was bigger than that for case N = 3. As exploitation progressed, the Q_{pr} for case N = 4 decreased and trended to stability, the Q_{pr} for cases N = 3 and N = 4 were similar. As shown in Q_{cv} curves, the Q_{cv} for case N = 5 was much bigger than that for cases N = 3 and N = 4, and case N = 4 was slightly bigger than case N = 3. This was because, dense fractured network had more cracks in fracturing zone, with a high-density fractured network, which had a better improvement effect for the permeability of NGH deposit. In comparison with cases N = 5 and N = 3, the Q_{cv} increased by 30.6%.

These results showed that, under low-permeability condition, the influence of dense fractured network on NGH conversion efficiency was most significantly, however, the influence were similar between dense and sparse fractured network, in low-permeability and low-saturation case.

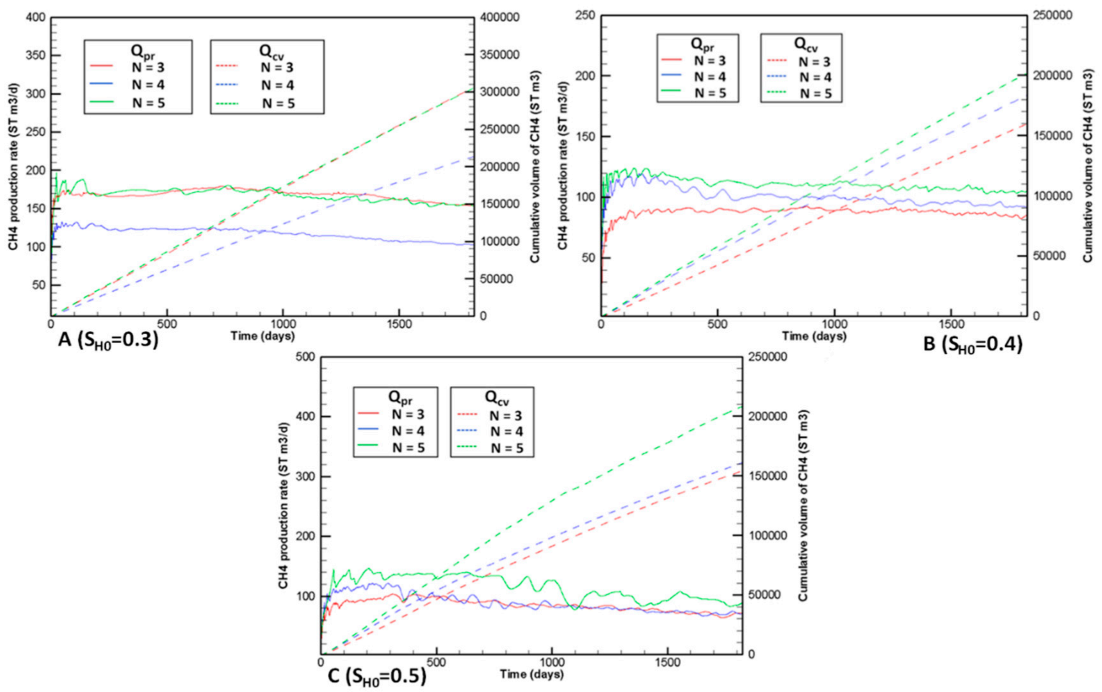

Fig. 3. Q_{pr} and Q_{cv} from NGH deposit in the Shenhu area under low-permeability (k=7.5mD) conditions in different N (N =3, 4, and 5).

Preprints (www.preprints.org) | NOT PEER-REVIEWED | Posted: 11 December 2017 doi:10.20944/preprints201712.0062.v1

Peer-reviewed version available at *Energies* **2018**, *11*, 339; doi:10.3390/en11020339

3.4.3. Analyze under High-Saturation Condition (S_{H0} = 0.5)

Fig. 4 and Fig.3C showed the CH_4 production rate Q_{pr} and the cumulative volume Q_{cv} curves under high-saturation (S_{H0} = 0.5) and different N conditions. By comparing the Q_{pr} curves of Fig.3C, Fig.4A and Fig.4B, under k = 7.5 mD and 40 mD conditions, the Q_{pr} for case N = 5 was bigger than that for cases N = 3 and 4 during the whole exploitation process, and Q_{pr} for cases N = 3 and 4 were similar. In high-permeability case, the Q_{pr} and Q_{cv} for case N = 3 were the largest.

In Fig. 4A, k = 40 mD. As shown in Q_{cv} curves, the Q_{cv} for case N = 5 was much bigger than that for cases N = 3 and N = 4, and the Q_{cv} for cases N = 3 and N = 4 were similar, and Q_{cv} increased by 14.1%, in comparison with cases N = 4 and N = 5. In Fig. 4B, k = 75 mD. As shown in Q_{cv} curves, the Q_{cv} for case N = 3 was the biggest, and the Q_{cv} for case N = 5 was bigger than that for case N = 4. The Q_{cv} increased by 21.3%, in comparison with cases N = 3 and N = 4.

This was because, Δl = 3m was the best spacing to increase the interaction between cracks, the Q_{pr} and Q_{cv} had the largest values in this spacing under the same crack quantity condition, also, a lower saturation led to a higher effective permeability, there were enough seepage channels to the discharge of methane to production well in high-permeability condition, therefore, the improvement of dense fractured network for high-permeability of NGH deposit was not obvious. However, in low-permeability case, dense fractured network had more cracks in fracturing zone, with a high-density fractured network, which had a better improvement effect for the permeability of NGH deposit.

These results showed that, under high-saturation condition, the influence of dense fractured network on NGH conversion efficiency was most significantly, however, the influence of sparse fractured network was better in high-permeability and high-saturation case.

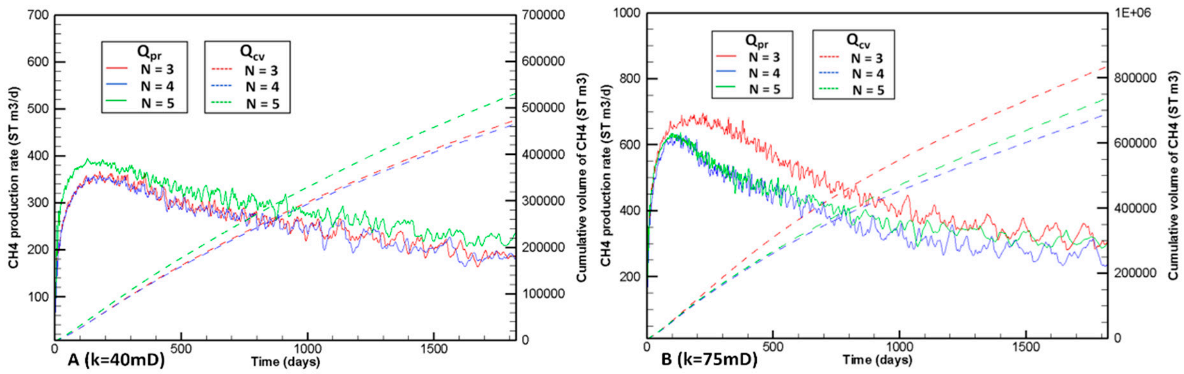

Fig. 4. Q_{pr} and Q_{cv} from NGH deposit in the Shenhu area under high-saturation (S_{H0} = 0.5) conditions in different N (N =3, 4, and 5).

3.4.4. Analyze under Other Accumulation Conditions

Fig. 5 showed the CH_4 production rate Q_{pr} and the cumulative volume Q_{cv} curves under other accumulation conditions. As showed in Q_{pr} curves of Fig. 5, in the early stage of exploitation, the Q_{pr} for case N = 5 was smaller than that for case N = 3, however, As exploitation progressed, the Q_{pr} for case N = 5 reached the stable value earlier, and the stable value for case N = 5 was larger than that for case N = 3. By comparing the Q_{pr} curves of Fig. 5, the higher permeability, the lower saturation, the earlier the Q_{pr} for case N = 5 exceeded case N = 3. This was because, under higher permeability and lower saturation conditions, there were more seepage channels to the discharge of methane to production well, and NGH dissociation area was closed to the production well in the early stage of exploitation, therefore, the improvement effect of dense fractured network for NGH deposit permeability was not obvious. As exploitation progressed, the improvement effect of dense fractured network was increased with increasing the distance between production well and decomposition front. And in higher permeability and lower saturation case, the NGH dissociation rate were faster.

In Fig. 5A, k = 40 mD, S_{H0} = 0.3. As shown in Q_{cv} curves, the Q_{cv} for cases N = 3 and N = 5 were

Preprints (www.preprints.org) | NOT PEER-REVIEWED | Posted: 11 December 2017 doi:10.20944/preprints201712.0062.v1

Peer-reviewed version available at Energies 2018, 11, 339; doi:10.3390/en11020339

similar and bigger than that for case N = 4 at five years, and the Q_{cv} increased by about 13.3%, in comparison with cases N = 3, N = 5 and N = 4. And as exploitation progressed, the Q_{cv} for cases N = 5 would bigger than that for case N = 3. In Fig. 5B, S_{H0} = 0.4. As shown in Q_{cv} curves, the Q_{cv} for case N = 3 was slightly bigger than that for case N = 5, and the Q_{cv} increased by 33.8%, in comparison with cases N = 4 and N = 3. In Fig. 5C, S_{H0} = 0.3. As shown in Q_{cv} curves, the Q_{cv} for case N = 5 was bigger than that for cases N = 3 and N = 4. And the Q_{cv} increased by 13.8%, in comparison with cases N = 5 and N = 4. In Fig. 5D, S_{H0} = 0.4. As shown in Q_{cv} curves, the Q_{cv} for cases N =3 and 5 were much bigger than that for case N = 4, and the Q_{cv} for cases N =5 was the largest. The Q_{cv} increased by 18.4%, in comparison with cases N = 4 and N = 5.

These results showed that, the influence of dense fractured network on NGH conversion efficiency was most significantly, under these accumulation conditions.

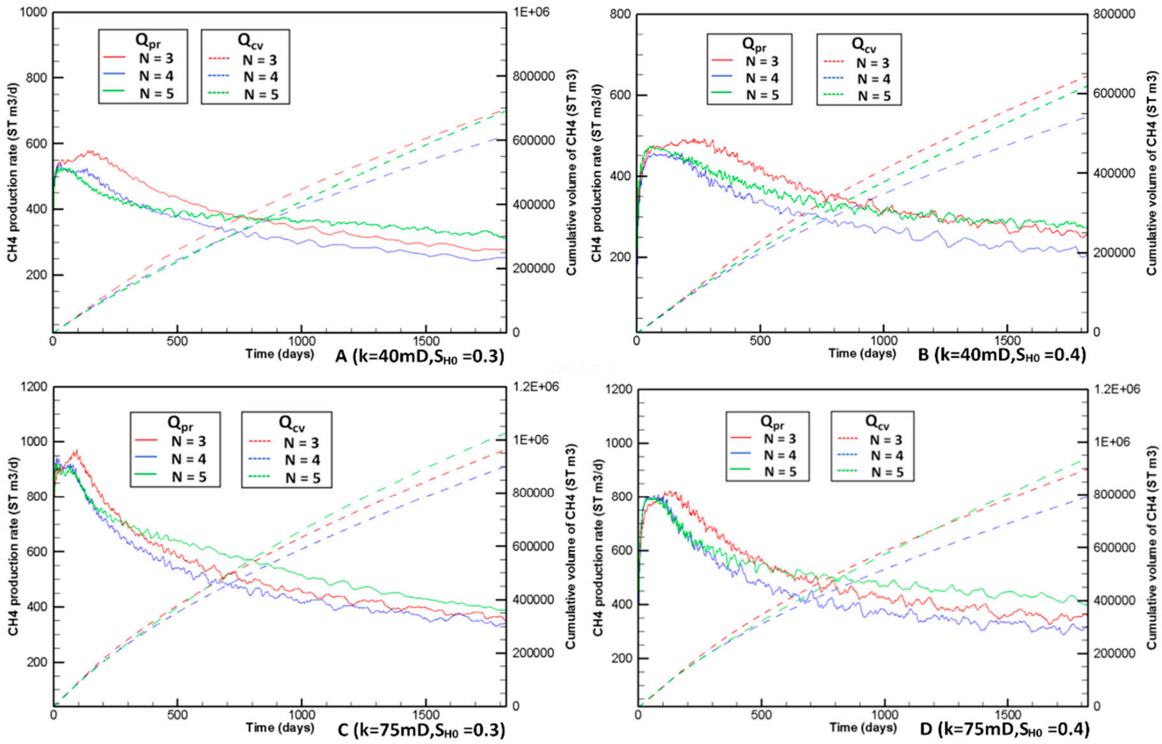

Fig 5. Q_{pr} and Q_{cv} from NGH deposit in the Shenhu area under different accumulation conditions in different N (N =3, 4, and 5).

4. Conclusions

In this paper, an NGH deposit in the Shenhu area, northern slope of the South China Sea area was simulated using TOUGH+HYDRATE v1.0 via RST and single vertical well depressurization method, based on the simulation results, the following conclusions were drawn:

1. Combining RST and single vertical well depressurization method to exploit NGH deposit under different intrinsic permeability and initial NGH saturation conditions, the sensitivity of stimulation effect on NGH conversion efficiency was significant, the sensitivity of intrinsic permeability was larger than that of initial NGH saturation, and the influence of interaction between these three factors were not obvious.
2. NGH conversion efficiency of stimulated NGH deposit was substantial increased with increasing intrinsic permeability, however, the growth rate was decreasing. A lower S_{H0} led to a higher NGH conversion efficiency of stimulated NGH deposit, and the reduction rate was decreasing. The influence on NGH conversion efficiency was increased by about 4 times, in comparison with initial NGH saturation and intrinsic permeability.

Peer-reviewed version available at *Energies* **2018**, *11*, 339; doi:10.3390/en11020339

3. The sensitivity of variably stimulation effect on NGH conversion efficiency were decreased with increasing initial NGH saturation and intrinsic permeability, respectively, and the sensitivity was most significantly under lower intrinsic permeability condition. The influence of intrinsic permeability on sensitivity of stimulation effect on NGH conversion efficiency was bigger than that of initial NGH saturation.
4. The stimulation effects required for a higher NGH conversion efficiency were different under different accumulation conditions. For loose fractured network, the influence was significant under higher permeability and saturation conditions. And under lower permeability and saturation conditions, the influence between loose and dense fractured network were similar. For other accumulation cases, dense fracture network had a significant influence.

It should be stressed here the conclusions above are based on pure numerical simulations. With the development of reservoir stimulation technique, it would be probably applied to exploit marine gas hydrate and improve the conversion efficiency, will greatly enlarge the potential use of NGH as a gas resource. Of course, it still need experimental verification that is under our right consideration. And in this work, we provide a reference program.

Acknowledgments: This study has been supported by National Natural Science Foundation of China (Grant No.41672361, Grant No. 41502343 and Grant No. 51474112), Scientific and Technological Development Program of Jilin Province (Grant No. 20170414044GH and Grant No. 20160204011SF), New energy projects (Grant No. SXGJSF2017-5), and Program for JLU Science and Technology Innovative Research Team (JLUSTIRT).

Author Contributions: Yang Lin analyzed the data and wrote the manuscript. Yang Lin, Chen Yong and Li Xitong performed the simulations. Jia Rui, Yang Lin and Chen Chen conceived the original ideas. All authors discussed the results and commented on the manuscript. Chen Chen, Sun Youhong and Guo Wei directed the overall project.

Conflicts of Interest: The authors declare no conflicts of interest.

References

1. Sloan ED; Koh CA. Clathrate Hydrates of Natural Gases, 3rd ed; CRC Press: Boca Raton, FL, USA, 2008.
2. Qorbani, K.; Kvamme, B.; Kuznetsova, T. Using a reactive transport simulator to simulate CH_4 production from bear island basin in the Barents Sea utilizing the depressurization method. *Energies* **2017**, *10*, 187.
3. Sun YH; Jia R; Guo W; Zhang YQ.; Zhu YH; Li B; Li K. Design and experiment study of the steam mining system for natural gas hydrates. *Energy Fuels* **2012**, *26*, 7280–7287.
4. Li YH, Song YC, Yu F, Liu WG, Zhao JF. Experimental study on mechanical properties of gas hydrate-bearing sediments using kaolin clay. *China ocean engineering* **2011**, *25*, 113-122.
5. Max MD; Johnson AH. Exploration and Production of Oceanic Natural Gas Hydrate: Critical Factors for Commercialization. Springer International Publishing AG: Basel, Switzerland, 2016; p. 405.
6. Ruan, X.; Li, X.S.; Xu, C.G. Numerical investigation of the production behavior of methane hydrate under depressurization conditions combined with well-wall heating. *Energies* **2017**, *10*, 161.
7. Johnson AH. Gas Hydrate In: GEA, 2011: The Global Energy Assessment. IIASA, Laxenburg; Austria and Cambridge University Press: Cambridge, UK; New York, NY, USA, 2012; pp. 35–43.
8. Lim JY, Kim E, Seo YW. Dual inhibition effects of diamines on the formation of methane gas hydrate and their significance for natural gas production and transportation. *Energy Convers Manage* **2016**, *124*, 578-586.
9. Max MD; Johnson AH. Diagenetic methane hydrate formation in permafrost: A new gas play? In Proceedings of the OTC Arctic Technology Conference, Houston, TX, USA, 7–9 February 2011.
10. Birkedal, K.A.; Hauge, L.P.; Graue, A.; Ersland, G. Transport Mechanisms for CO_2-CH_4 Exchange and Safe CO_2 Storage in Hydrate-Bearing Sandstone. *Energies* **2015**, *8*, 4073–4095.
11. Max MD; Johnson AH. 2011. Methane Hydrate/Clathrate Conversion. In Clean Hydrocarbon Fuel Conversion Technology, Woodhead Publishing Series in Energy No. 19; Khan, M.R., Ed.; Woodhead Publishing Ltd.: Cambridge, UK; pp. 413–34; ISBN 1 84569 727 8, ISBN-13: 978 1 84569 727 3.
12. Konno Y, Masuda Y, Akamine K, Naiki M, Nagao J. Sustainable gas production from methane hydrate reservoirs by the cyclic depressurization method. *Energy Convers Manage* **2016**, *108*, 439-445.
13. Wang B; Huo P; Luo T; Fan Z; Liu FL; Xiao B; Yang MJ; Zhao JF; Song YC. Analysis of the Physical Properties of Hydrate Sediments Recovered from the Pearl River Mouth Basin in the South China Sea: Preliminary Investigation for Gas Hydrate Exploitation. *Energies* **2017**, *10*, 531.

14. Li G; Moridis GJ; Zhang K; Li XS. Evaluation of NGH conversion potential from marine gas hydrate deposits in Shenhu area of South China Sea. *Energy Fuels* **2010**, *24*, 6018–6033.
15. Zhang W; Liang JQ; Lu JA; Wei JG; Su PB; Fang YX; Guo YQ; Yang SX; Zhang GX. Accumulation mechanisms of high saturation natural gas hydrate in Shenhu Area, northern South China Sea. *Petroleum exploration and development* **2017**, *44*, 1-11.
16. He JX; Yan W; Zhu YH; Zhang W; Gong FX; Liu SL; Zhang JR; Gong XF. Bio-genetic and sub-biogenetic gas resource potential and genetic types of natural gas hydrate in the northern marginal basins of South China Sea. *Nat. Gas Ind.* **2013**, *33*, 121-134.
17. Su M; Yang R; Wu NY. Structural characteristics in the Shenhu Area, northern continental slope of South China Sea, and their influence on gas hydrate. *Acta Geologica Sinica* **2014**, *88*, 318-326.
18. Liang JQ; Wang HB; Su X. Natural gas hydrate formation conditions and the associated controlling factors in the northern slope of the South China Sea. *Nat. Gas Ind.* **2014**, *34*, 128-135.
19. McDonnell SL; Max MD; Cherkis NZ; Czarnecki MF. Tectono-sedimentary controls on the likelihood of gas hydrate occurrence near Taiwan. *Mar. Pet. Geol*. **2000**, *17*, 929-936.
20. Guo YQ; Yang SX; Liang JQ; Lu JA.; Lin L; Kuang ZG. Characteristics of high gas hydrate distribution in the Shenhu Area on the northern slope of the South China Sea. *Earth Science Frontiers* **2017**, *24*, 24-31.
21. Yang SX; Liang JQ; Liu CL; Sha ZB. Progresses of gas hydrate resources exploration in sea area. *Geological Survey of China* **2017**, *4*, 1-8.
22. Su Z; Li H; Wu NY; Yang SX. Effect of thermal stimulation on NGH conversion from hydrate deposits in Shenhu area of the South China Sea. *Earth Sci.* **2013**, *56*, 601–610.
23. Chen C; Yang L; Jia R; Sun YH; Guo W; Chen Y; Li XT. Simulation study on the effect of fracturing technology on the production efficiency of natural gas hydrate. *Energies* **2017**, *10*, 1241.
24. Wu Q; Xu Y; Liu YZ; Ding YH; Wang XQ; Wang TF.The current situation of stimulated reservoir volume for shale in U.S. and its inspiration to China. *Oil Drill. Product. Technol.* **2011**, *33*, 1–7.
25. Lancaster DE; Holditch SA; Mcketta SF; Hill RE; Guidry FK; Jochen JE. Reservoir evaluation, completion techniques, and recent results from Barnett shale development in the fort worth basin. In Proceedings of the SPE Annual Technical Conference and Exhibition, Washington, DC, USA, 4–7 October 1992.
26. Li Y; Cao G. Development technology for low-permeability sandstone reservoirs in Shengli Oil field. *Pet. Explor. Dev.* **2005**, *32*, 123–126.
27. Wu Q; Xu Y; Wang TF; Wang XQ. The revolution of reservoir stimulation: An introduction of volume fracturing. *Nat. Gas Ind.* **2011**, *31*, 7–12.
28. Zhang YJ; Li ZW; Guo LL; Gao P; Jin XP; Xu TF. Electricity generation from enhance geothermal systems by oilfield produced water circulating through reservoir stimulated by staged fracturing technology for horizontal wells: A case study in Xujiaweizi area in Daqing Oilfield, China. *Energy* **2014**, *78*, 788–805.
29. Sun YH; Li B; Wei G. Comparative Analysis of a Production Trial and Numerical Simulations of NGH conversion from Multilayer Hydrate Deposits in the Qilian Mountain Permafrost. *J. Nat. Gas Sci. Eng.* **2014**, *21*, 456–466.
30. Song Y; Zhang L; Lv Q; Yang M; Ling Z; Zhao J. Assessment of NGH conversion from natural gas hydrate using depressurization, thermal stimulation and combined method. *RSC Adv.* **2016**, *6*, 47357–47367.
31. Qorbani K; Kvamme B. Non-equilibrium simulation of CH_4 production from gas hydrate reservoirs through the depressurization method. *J. Nat. Gas Sci. Eng.* **2016**, *35*, 1544–1554.
32. Moridis GJ; Kowalsky MB; Pruess K. TOUGH+HYDRATE v1.0 User's Manual: A Code for the Simulation of System Behavior in Hydrate-Bearing Geologic Media; Lawrence Berkeley National Laboratory: Berkeley, CA, USA, 2008.
33. Moridis GJ, Seol Y, Kneafsey TJ. Studies of reaction kinetics of methane hydrate dissociation in porous media. In The 5th International Conference on Gas Hydrate, Trondheim, Norway, 2005, pp.1004.
34. van Genuchten MT. A closed-form equation for predicting the hydraulic conductivity of unsaturated soil. *Soil Sci. Soc. Am. J.* **1980**, *44*, 892-898.
35. Li G; Li XS; Chen Q; Chen ZY. Numerical simulation of NGH conversion from gas hydrate zone in Shenhu are, South China Sea. *Acta Chimica Sinica* **2010**, *68*, 1083–1092.
36. Phillips OM. Flow and Reactions in Permeable in Permeable Rocks; Cambridge University Press: Cambridge, UK, 1991.
37. Verma A; Pruess K. Thermohydrologic conditions and silica redistribution near high-level nuclear wastes emplaced in saturated geological formations. *J. Geophys. Res.* **1988**, *93*, 1159–1173.
38. Xu T; Ontoy Y; Molling P; Spycher N; Parini M; Pruess K. Reactive transport Modeling of injection well scaling and acidizing at Tiwi field, Philippines. *Geothermics* **2004**, *33*, 477–491.